GA–A27171

THE GENERAL ATOMICS FUSION THEORY PROGRAM REPORT FOR GRANT YEAR 2011

by
PROJECT STAFF

NOVEMBER 2011

GENERAL ATOMICS

DISCLAIMER

GA–A27171

THE GENERAL ATOMICS FUSION THEORY PROGRAM REPORT FOR GRANT YEAR 2011

by
PROJECT STAFF

Work supported by
the U.S. Department of Energy
under Grant No. DE-FG03-95ER54309

GENERAL ATOMICS PROJECT 03726
NOVEMBER 2011

ABSTRACT

The objective of the fusion theory program at General Atomics (GA) is to significantly advance our scientific understanding of the physics of fusion plasmas and to support the DIII-D and other tokamak experiments as well as ITER research activities. The program plan is aimed at contributing significantly to the Fusion Energy Science, the Tokamak Concept Improvement, and ITER goals of the Office of Fusion Energy Sciences (OFES). Significant progress was made in each of the important areas of our research program during the last grant period GY11. This includes: continued development of the EPED predictive models for the H-mode pedestal height and width and its successful validation against tokamak experimental data, as part of the 2011 Joint Research Target (JRT) on pedestal structure; demonstration with a set of two-fluid M3D-C1 MHD simulations of DIII-D equilibria that error-field penetration is greatest when the perpendicular electron velocity is close to zero; demonstration with a set of NIMROD DIII-D MHD simulations that the runaway-electron confinement times vary with the magnetic field fluctuation amplitudes as predicted by the Rechester-Rosenbluth model; formulation of GYRO to include model external and static magnetic perturbations in gyro-kinetic turbulent transport simulations and its applications; demonstration with GYRO energetic particle simulations that a RSAE mode transits to a TAE mode as the core safety factor evolves consistent with DIII-D experimental observations; demonstration with a set of TGLF simulations of recent DIII-D experiments that the electron transport is very stiff while the ion transport is only moderately stiff; evaluation of the physical accuracy and limitations of several commonly used model collision operators using the new NEO upgraded full Fokker-Planck collision operator; and installation of a version of the IMFIT integrated modeling tool at ASIPP-Hefei and IPR-India to support EAST and SST-1 analysis and modeling.

TABLE OF CONTENTS

1. HIGHLIGHTS OF THEORY WORK IN GY11

During the past grant year, significant progress was made in each of the important areas of our research program:

- Successful comparison of the EPED1 model against a set of DIII-D discharges as part of the 2011 Joint Research Target (JRT) on pedestal structure with a ratio of predicted to observed pedestal height of 1.00 ± 0.06.
- Study of a recent DIII-D experiment to rigorously test the EPED1.6 model and kinetic ballooning mode physics finds good agreement between the EPED1.6 model and the observed pedestal structure over a wide range of pedestal height and width.
- Analytic analysis of symmetries of the MHD fluid equations under the reversal of toroidal field, current, and rotation showing that ideal, resistive, and two-fluid terms each possess distinct symmetry groups.
- Derivation of a formula for the partial helicity that includes the twist, torsion, and writhe contributions within a given magnetic surface for intact flux surfaces in a 3D toroidal system.
- Implementation of a new capability to the 3D MHD code M3D-C1 to perform time-independent calculations of linear plasma response by dynamically advancing the system that significantly reduce the computational cost for stable equilibria.
- Demonstration with a set of two-fluid M3D-C1 simulations of DIII-D equilibria that error-field penetration is greatest when the perpendicular electron velocity is close to zero.
- Successful non-linear calculations of 3D plasma response to externally applied non-axisymmetric fields for a DIII-D discharge and an ITER model equilibrium using M3D-C1 at low resolution.
- Demonstration with NIMROD simulations that differences in the initial equilibrium current profiles and not the pellet ablation are responsible for the different run-away currents observed in a DIII-D Ar pellet disruption mitigation experiment.
- Demonstration that the runaway-electron confinement times vary with the magnetic field fluctuation amplitudes as predicted by the Rechester-Rosenbluth model with a set of 3D NIMROD simulations of mitigated disruptions in DIII-D that includes drift-motion calculation for a test population of runaway electrons.
- Demonstration using the 3D MHD code NIMROD that in a DIII-D massive gas injection disruption mitigation experiment as the MHD modes saturate, rapid parallel heat transport along stochastic fields begins to cool the core.

- Formulation of GYRO to include model external and static magnetic field perturbations for studies of their effects on transport from the deflection of the parallel magnetic field direction.
- Completion of a theoretical formulation for a version of GYRO suitable for the strongly collisional pedestal region.
- Demonstration with a set of GYRO simulations that the spectral average radial wave number of the non-linear electric potential depends linearly on the local mid-plane magnetic shear with no dependence on the safety factor.
- Demonstration with electromagnetic global GYRO simulations of the near edge region for two DIII-D L-mode discharges at very expensive short spatial scales that short radial-scale micro-tearing modes do not lead to increased transport.
- Demonstration that it may be possible to construct a model to relate the turbulent radial conductivity of an externally isolated island to the radial current flux through the island with a study of GYRO simulations that include external resonant magnetic perturbations.
- Demonstration with GYRO simulations that in spherical tokamaks electron thermal transport is comparable to that given by experimental analysis and is dominated by the electromagnetic contribution of electrons free streaming along the stochastic magnetic field lines.
- Identification of a global reverse-shear Alfvén eigenmode (RSAE) in GYRO simulations of a DIII-D discharge with a visible characteristic frequency upsweep.
- Demonstration with GYRO simulations of global Alfvén eigenmodes that a transition from a single poloidal mode-number m RSAE to a two-m TAE as the core safety factor evolves consistent with ECE measurements in a DIII-D discharge.
- Formulation of the TGLF moment equations for large Mach number that may enhance the momentum transport in the presence of an internal transport barrier.
- Completion of a sensitivity study of more than 25 DIII-D L-mode discharges showing that TGLF systematically under-predicts the energy transport in the near edge region for both the electron and ion channels.
- Development of an improved model for the radial wave number in TGLF based on the spectral average wave number that significantly improves agreement between TGLF and GYRO toroidal stress and fluxes when both a parallel and a Doppler shear are present.
- Completion of a study to quantify the stiffness of TGLF transport in a number of DIII-D L- and H-mode discharges (defined as ratio of the normalized change in

transported power to the change in temperature gradient) that shows several intertesting trends including a very weak dependence on the β values.

- Demonstration that the electron transport is very stiff while the ion transport is only moderately stiff with a set of TGLF modeling studies of recent DIII-D experiments explicitly designed to study the stiffness of the core transport in H-mode plasmas.
- Implementation of a full linearized Fokker-Planck collision operator in NEO using new numerical algorithms designed for high-accuracy implicit evaluation of multi-species plasmas.
- Evaluation of the physical accuracy and limitations of several commonly used model collision operators using the new upgraded full Fokker-Planck collision operator implemented in the NEO code.
- Improvement of the quasi-linear heating operator in ORBIT-RF by including the effects due to change in parallel velocity in the fast Alfvén waves absorption by particles.
- Development of analytical expressions for the time dependence of many high-pressure gas flow dynamic variables that agree well with 2D asymmetric FLUENT simulations for sufficiently high conductance pipes in valve-limited flows.
- Installation of a version of the IMFIT integrated modeling tool at ASIPP-Hefei and at IPR-India to support EAST and SST-1 analysis and modeling.
- Extraction and development of the NFREYA neutral beam module from the ONETWO transport code into an independent parallel module to support the new DIII-D off-axis neutral-beam operation.
- Development of a new version of the ONETWO transport code that includes the new parallel version of the neutral beam module PNFREYA and a number of significant enhancements to the ONETWO plasma state file.
- Development of a driver module to integrate and run the GENRAY RF package under the IMFIT framework.

As a consequence of these results, scientists from the Theory Group were selected to give a number of invited talks and colloquia as highlighted in the next section. Sections 3–6 provide more detailed descriptions of the advances and achievements made in each of the major areas. A list of publications is given in Section 7.

2. SIGNIFICANT PRESENTATIONS IN GY11

2011 PRESENTATIONS

53RD APS DPP meeting in Salt Lake City, Utah November 14–18, 2011:

- N.W. Ferraro gives an invited presentation "Calculation of Linear Two-Fluid Plasma Response to Applied Non-Axisymmetric Fields."
- P.B. Snyder gives an invited presentation "The EPED Pedestal Model: Extensions, Experimental Tests, and Application to ELM-suppressed Regimes."

FSP Definition Workshop in San Diego, CA February 8-11, 2011:

- V.S. Chan gave a presentation "FSP Experimental Validation Overview."
- P.B. Snyder gave two presentations "The Pedestal Science Driver: Science Goals, Plan, and User Cases" and "Pedestal Validation: Examples of Current Practice and 3-5 Year Vision."

US-Japan RF Physics Workshop in Toba, Japan February 8-9 2011:

- M. Choi gave a presentation "Previous and Ongoing Benchmarking Activities on Self-Consistent ICRH Modeling."

ITPA Pedestal Topical Meeting in Cambridge, MA March 30 – April 1, 2011:

- N.W. Ferraro gave a presentation "Linear Stability and Response Calculations with Resistivity, Rotation, and Two-Fluid Effects."
- P.B. Snyder gave a presentation "Progress in the EPED Pedestal Model: Comparison to Hybrid and Baseline Discharges on JET."

Joint EU-US Transport Task Force Workshop in San Diego, CA April 6–9 2011:

- P.B. Snyder gave a presentation "Developing and Testing the EPED Pedestal Model: Comparisons to Hybrid and Baseline Discharges on JET."

Stochasticity in Fusion Plasmas Workshop in Julich, Germany April 11–14, 2011:

- A.D. Turnbull gave an oral presentation "Plasma Response Models for Non-Axisymmetric Perturbations."

19TH Topical Conference on Radio Frequency Power in Plasmas in Newport, Rhode Island June 1–3, 2011:

- M. Choi gave a presentation "Modeling of Synergy between 4^{th} and 6^{th} Harmonic Absorptions of Fast Waves on Injected Beams in DIII-D Tokamak."

38TH European Physical Society Conference on Plasma Physics in Strasbourg, France June 27–July 1, 2011:

- G.M. Staebler gave an oral presentation "Multispecies Gyro-Kinetic Momentum Transport Modeling with the Trapped Gyro-Landau Fluid Model."

Integrated Technology Workshop at ITER Headquarters Cadarache, France June 8–10, 2011:

- L.L. Lao gave a presentation "Automated Reconstruction and Experimental Integrated Modeling and Data Analysis in DIII-D."

SciDAC 2011 Workshop in Denver, CO July 14, 2011:

- N.W. Ferraro gave an invited oral presentation "Fluid Modeling of Fusion Plasmas with M3D-C1."

3. ADVANCES IN MHD EQUILIBRIUM AND STABILITY RESEARCH

3.1. 3D EQUILIBRIUM STATES

Role of Helicity in 3D Equilibria Transformations: Progress was made on understanding the role of helicity in equilibria undergoing transformations. A formula for the partial helicity within any given magnetic surface was derived that can be calculated easily in the axisymmetric case. A similar but more general expression can also be calculated for intact flux surfaces in the non-axisymmetric system. Expressions for the helicity were also calculated for model cases and shown to reduce to the correct expressions for cases of linked spatially separated flux tubes. The physics of helicity in terms of the contributions from twist, torsion, and an inherent helicity describing the twistedness of the core field line of a flux tube, also called the 'writhe', is better understood. Though the twist, torsion, and writhe contributions are not independently conserved by ideal motions, they can be calculated in principle for non-nested regions to yield the partial helicity over those regions.

The helicity was calculated explicitly for a commonly used model q profile and was shown to reduce at large radius to a product of the toroidal and poloidal fluxes and an effective linking number. The helicity also vanishes explicitly for a linear q-profile, thus highlighting the role of shear.

3.2. PEDESTAL MODEL DEVELOPMENT, VALIDATION, AND ANALYSIS

EPED Pedestal Model Analysis: The EPED1 model has been successfully compared to a large dataset of experiments on JET, DIII-D and AUG. Agreement between the predicted and observed pedestal height on all three machines is found to be quite good, as shown in Fig 1.

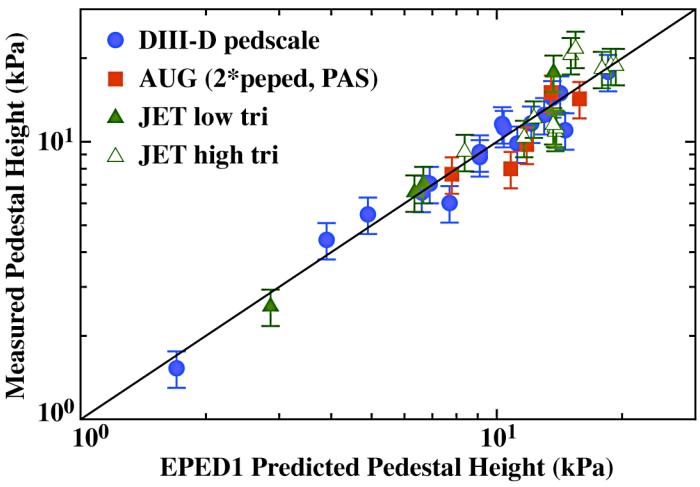

Fig. 1. Comparison of EPED1 predictions of the pedestal height to observations on JET, DIII-D, and AUG. Good agreement is found across all three devices.

A set of experiments was conducted on Alcator C-Mod to test the EPED pedestal model. These experiments were carried out with P. Snyder serving as co-session leader with J. Hughes. A current scan in ELMing discharges was extended to include data at 650 kA, 750 kA, 900 kA and 1 MA. On two separate experimental days, a shape scan was conducted, varying the elongation while remaining in ELMing H-mode. Higher pedestals at higher elongation were observed as predicted by the EPED model. This work was conducted in support of the 2011 Joint Research Target on pedestal structure.

Additionally, the EPED1 model has been successfully compared to a full dataset of 137 baseline and hybrid discharges on JET. This comparison to the full set of analyzed JET discharges finds good agreement with the EPED1 model, with a ratio of predicted to observed pedestal height of 0.97 ± 0.21, with a correlation coefficient of 0.86. This level of correlation between the model and observation is found to be consistent with a model accuracy of 20% or better (with no free parameters). Similar levels of agreement are found with hybrid and baseline discharges and with high and low triangularity cases.

The EPED1 model has been also compared to a set of DIII-D discharges as part of the 2011 Joint Research Target (JRT) on pedestal structure. A set of DIII-D discharges containing a current scan were carefully analyzed as part of the JRT to yield accurate measurements of pedestal structure. A comparison with the EPED1 model found excellent agreement, with a ratio of predicted to observed pedestal height of 1.00 ± 0.06 in these four cases.

A study of discharges where ELMs are suppressed with resonant magnetic perturbations (RMP) has also been performed using the EPED model. The goal is to characterize criteria for stabilization of ELMs and further develop a working model for ELM suppression. The EPED1 model has also been run on a set of more than 400 randomly generated DIII-D-like cases. The goal is to assemble a large database of EPED results that can be parameterized for ease of use in experimental planning and control room analysis

New DIII-D Experiment to Test EPED and Kinetic Ballooning Mode Physics: An experiment has been conducted on DIII-D to rigorously test the EPED model and kinetic ballooning mode (KBM) physics over a wide range of parameters. The experiment takes advantage of a newly upgraded Thomson scattering system on DIII-D to provide both higher spatial and temporal resolution measurements of profiles across the edge barrier. The EPED model was used to predict the pedestal height and width before the experiment was conducted, and an initial study has found good agreement between the model and the observed pedestal structure, over a wide range of pedestal height and width. Fluctuation measurements using the BES and DBS diagnostics find high frequency modes that rise up during the latter half of the ELM cycle in several discharges. Further analysis of this experiment and comparisons to the EPED model and direct gyro-kinetic calculations are ongoing in preparation for an APS/DPP invited talk.

3.3. PLASMA RESPONSE TO EXTERNAL PERTURBATION FIELDS

Analytic Study of 3D Plasma Response: An analytic analysis of symmetries of fluid equations under the reversal of toroidal field, current, and rotation has shown that ideal, resistive, and two-fluid terms each possess distinct symmetry groups. This finding may allow for the determination of the dominant physical processes involved in a phenomenon through a series of experiments in which the field, current, and rotation reversed in various combinations.

A much better understanding of the issues and theory behind the response of a plasma to an external perturbation was also obtained. Changes in stability always, and can only, occur at bifurcation points as a parameter is varied. The distinction between adiabatic and non-adiabatic evolution as a plasma parameter is varied through a bifurcation (and therefore stability) point was also clarified. The available solutions depend on the type of bifurcation (turning point, pitchfork, or Hopf bifurcation) crossed and this can be determined in principle by a local analysis. The differences between the response to an internal instability and an external perturbation can be subtle and depend on whether evolution of the plasma parameters is adiabatic or not. The relation of the various approaches to the Reiman model was also clarified: in particular, the Reiman model explicitly invokes a slowly varying non-axisymmetric perturbation as the parameter being varied.

The relation between various different approaches to the plasma response was also clarified. A direct relation was found between forced oscillation dynamics approach and the eigenvalue expansion approach for the linear case in terms of the Greens Function. The linear approach provides the direction of steepest gradient in the energy landscape and therefore a direction for the determination of the lower energy final nonlinear state. Also the relation of the nonlinear nearby equilibrium approach to the original Almost Ideal MHD approach of Jensen was better clarified. The relation between the symmetries imposed by available 3D equilibrium codes and constraints on the final states was made more explicit.

M3D-C1 Development: The capability to perform time-independent calculations of linear plasma response has been added to M3D-C1. This capability differs from the previous method of obtaining time-independent response by advancing the system dynamically until steady-state is reached. For stable equilibria, the new method obtains essentially the same result at a much lower computational cost. The utility of a time-independent method of calculating nonlinear non-axisymmetric steady states is less certain because of the non-uniqueness of nonlinear solutions, and is being evaluated.

Several additional capabilities have also recently been implemented in M3D-C1 that will aid future non-axisymmetric response calculations. First, non-axisymmetric field data generated by the PROBE_G code using actual coil geometries may now be directly imported into M3D-C1. Second, M3D-C1 may now optionally represent fields generated from external currents separately from fields generated from plasma currents. Current densities associated

with the external fields are excluded from the model equations. This allows non-axisymmetric coils to be present within the computational domain without causing numerical difficulties, which is necessary when using accurate vacuum vessel shapes. Finally, a number of numerical methods within M3D-C1 have been reformulated, resulting in a reduction in time-to-solution of up to 20% in some cases.

M3D-C1 Non-axisymmetric Plasma Response: The two-fluid linear response of diverted DIII-D equilibria to applied n=1 I-coil fields has been calculated using M3D-C1, yielding several interesting results. In particular, it was found that error-field penetration is greatest when the perpendicular electron velocity is close to zero, in agreement with recent two-fluid results obtained in straight-cylindrical geometry (Fig. 2). Furthermore, rotational screening was found to be a function of not only the magnitude, but also the direction, of rotation, even within the context of single-fluid MHD. This asymmetry is attributed to the up-down asymmetry of the equilibrium and the inherent helicity of the applied field. Strong rotation near the H-mode pedestal may excite sub-marginal edge modes, leading to increased stochasticity there. In all cases, parallel resonant "screening" currents were found to exist in thin boundary layers near the mode-resonant surfaces even in the time-independent steady state.

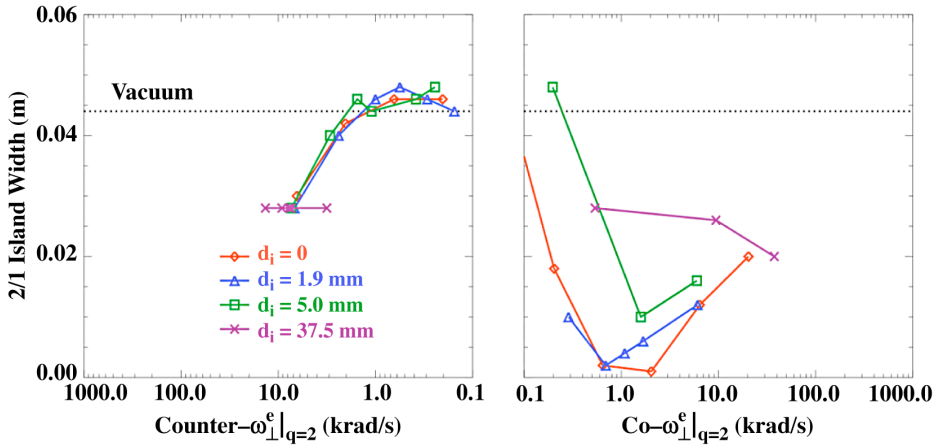

Fig. 2. The 2/1 island width due to the application of a 10 kA n=1 I-coil applied field, including two-fluid linear plasma response, for a low-β DIII-D equilibrium. The penetration is greatest near the point where the perpendicular electron rotation is zero.

An analysis of the linear plasma response of several reconstructed DIII-D equilibria has been carried out. In particular, shot 126006 has been studied in some detail. One goal of these calculations was to quantify the expected magnetic response near the separatrix, to determine whether it is large enough to observe clearly with a plunging magnetic probe. These calculations were also carried out by M. Lanctot using MARS-F. Both codes showed comparable response, of up to 5–10 G/kA just within the separatrix. Another goal of these calculations was to estimate the "displacement" of the magnetic surfaces under the actions of the non-axisymmetric fields. Calculations of this displacement were also undertaken by E. Lazarus and M. Lanctot using VMEC and MARS-F, respectively. The results of the

VMEC and MARS-F calculations are found to differ significantly. The M3D-C1 results were found to more closely resemble the MARS-F results. The source of the remaining discrepancies is a subject of ongoing research.

M3D-C1 Non-Linear Plasma Response: Fully nonlinear three-dimensional calculations have been carried out for the first time using M3D-C1, following recent improvements in the meshing software under development at RPI. M3D-C1's use of Hermite elements in the toroidal direction confers two potential advantages over the use of Fourier modes: the capability for non-uniform resolution in the toroidal direction, and a block tri-diagonal matrix structure, which may be factorized more efficiently. Preliminary calculations testing these capabilities include a sawtooth calculation in which the self-consistent heating, current evolution, and subsequent sawtooth crash are simulated over more than ten sawtooth cycles. Software libraries on which M3D-C1 depends have now been installed on Hopper, and M3D-C1 has been found to scale well to several thousand processes.

Preliminary nonlinear calculations of non-axisymmetric response have also been carried out. In particular, the fully nonlinear, non-axisymmetric equilibrium of DIII-D shot 126006 and an ITER 15 MA model equilibrium, subject to externally applied non-axisymmetric fields, have been calculated, using Spitzer resistivity. These calculations, which require substantially more computational resources than linear calculations, have only been carried out at relatively low resolution so far.

NIMROD Simulations of DIII-D L-Mode RMP Discharges: A set of NIMROD simulations has been run for two L-Mode DIII-D discharges in which n=1 applied C-coil fields of 1 and 3 kA were applied. In these DIII-D discharges, direct probe measurements of various quantities were made in the outer few cm of the plasma both before and after the C-coil fields were applied. Vacuum fields calculations in each case indicate the presence of a large 3/1 island that is intersected by the probe. In NIMROD plasma response calculations, the large 3/1 island remains, but is slightly screened by rotation and also phase shifted as predicted by error-field theory. With respect to validation of probe data, the phase shift of the island o-point away from the probe location is a significant effect. In the simulations, a reduction in density at the probe location is seen which is in qualitative agreements with the measurements. In the simulation the flattening of the temperature profile at the 3/1 island produces a slight temperature increase on the outboard side of the island, whereas the measured edge T_e in the DIII-D experiments decreases. A number of factors may be responsible for the discrepancy, most relating to limitations in the NIMROD transport model.

3.4. DISRUPTION MODELING

Effects of Applied Electric Field on Runaway Electron Currents: A 0.5-D model was developed in the last quarter to simulate the effects of radial transport or direct orbit loss of the runaway electrons (RE) to the vessel wall on the dissipation of the RE current. Analytical limits when the runaways are carrying the full current ("plateau-phase" or fully avalanched

mature runaways) were obtained. The 0.5 D model is good agreement with the 1D Grad-Shafranov model for a fully dominated RE discharge for downward RE current ramps.

NIMROD Disruption and Runaway Electron Modeling: NIMROD simulation results of two diverted DIII-D discharges terminated by Ar pellet injection have been compared to examine the factors associated with production of a large runaway-electron (RE) current plateau in DIII-D. DIII-D diverted RE experiments produce RE current plateaus very unreliably on a shot-to-shot basis, which motivated a GATO stability analysis of these discharges after Ar pellet injection, at the start of the thermal quench (TQ). That study found that those discharges that were unstable to on-axis peaked n=1 modes had low RE currents after the TQ, whereas off-axis peaked modes were correlated with high RE currents. NIMROD simulations of two discharges having high and low RE currents were run starting with equilibria prior to Ar pellet injection, and using a simplified Ar cooling model. NIMROD results agreed with GATO regarding the on/off-axis peaking of the initial unstable mode in each case, and also found much greater RE losses in the on-axis peaked case, in agreement with the experimental result of low RE current. These results specifically suggest that differences in the initial equilibria and not the pellet ablation produce the different RE current results.

In the DIII-D simulations, the escaping electrons striking the outer divertor early in time, and the main chamber later in time, which appears consistent with the experiments. The NIMROD radiated power spike at the time of the MHD onset has quantitative similarity to the radiated power spike in DIII-D, and the total radiated energy during the disruption shows a very close match between simulation and experiment.

With a greater number of electron orbits, the electrons can be weighted to the grid to obtain continuum quantities for visualization purposes. Contours of synchrotron radiation brightness have been produced to compare directly with DIII-D fast-camera images of runaway-electron beams. A synthetic diagnostic that accounts for camera viewing angle and frequency response could be created from this data for better validation.

NIMROD Runaway Electron Confinement Studies: NIMROD has been used to model rapid shutdowns by Ar pellet injection in six diverted DIII-D discharges, to investigate the wide variability of RE confinement seen for diverted plasma shapes on a shot-to-shot basis. The simulations can predict variations in MHD de-confinement due to current profile differences in the initial equilibrium, and distinguish these effects from variations in the pellet ablation, which may exist experimentally. The predicted RE confinement in the simulations correlates well with the observed RE current in the experimental discharges, with only one exception. For the four simulations having $q_0 < 1$, the MHD fluctuations have the same radial structure with only the amplitude varying. The RE confinement times in these cases vary with fluctuation amplitude in the manner predicted by the Rechester-Rosenbluth model, and the amplitude appears to be determined by the value of q_{95}. The two $q_0 > 1$ cases have qualitatively different behavior, but additional simulations are needed to determine what properties of those equilibrium affect RE confinement.

NIMROD Simulations of Massive Gas injection (MGI): A simulation of neon massive gas injection (MGI) into DIII-D was carried out with the NIMROD code. A source of neutral neon localized to the edge was specified, which cooled the edge until MHD instabilities were triggered. As the MHD modes saturate, rapid parallel heat transport along stochastic fields begins to cool the core. But the core temperature then rapidly drops to its current quench (CQ) value of 4 eV due to convection associated with an m=1/n=1 instability. The flows associated with the 1/1 mode also very efficiently mix Ne ions from the edge into the core. In another simulation, argon MGI into a low-elongation Alcator C-Mod plasma was modeled, to study runaway electron (RE) confinement. As was the case for low-elongation DIII-D plasmas, RE confinement was found to be better than for high-elongation plasmas, which is consistent with experimental results on both devices.

3.5. IDEAL AND TEARING STABILITY MODELING

DIII-D Ideal Stability Analysis: Calculations of a DIII-D AT discharge using GATO found complete stability for n=1, 2, and 3 modes with no wall, in contrast to DCON calculations that indicate this discharge is above the no-wall limit. The discrepancy has been traced to significant differences between the original reconstructed EFIT equilibrium used in the GATO study and the equilibrium calculated using CORSICA and TEQ used in DCON. When the latter equilibrium is used in GATO, the code does find instability. Thus, there is a significant difference between the CORSICA modeling of the equilibrium and the EFIT reconstruction. From additional GATO runs with the CORSICA equilibrium used by DCON, part of the difference is the smoothing that CORSICA uses at the edge to force the current density to vanish smoothly there. There is an additional discrepancy that DCON is apparently finding an internal mode for this case. Tests are underway with GATO at high resolution with additional strong packing to determine if there is an underlying internal second mode in the CORSICA equilibrium but the preliminary results indicate this is unlikely.

NIMROD Simulations of DIII-D Counter-ECCD Driven Tearing Modes: NIMROD has been used to model a DIII-D experiment in which a 3/2 tearing mode was driven with counter-ECCD. A simulation started with an equilibrium time-slice prior to the ECCD confirms the plasma is initially stable to all modes at the q=3/2 surface. Once the ECCD is turned on, the reconstructed equilibrium exhibits a small current deficit around q=3/2, which drives unstable modes in the nonlinear simulations. With a small number or toroidal mode numbers retained in the simulation (n=0–5) the m=3/n=2 mode grows and saturates as expected. However, with more toroidal modes included in the calculation, higher-n instabilities with q≈3/2 become dominant over the n=2 (although n=2 is still initially the fastest growing mode). For instance, with n=0–21 retained, the n=20 component is the largest mode in the nonlinear phase, with poloidal mode numbers m=29–31. In this case, a stochastic region appears near q=3/2 instead of an island. The high-n modes in reality may be stabilized by effects not included in these resistive MHD calculations.

4. ADVANCES IN TRANSPORT RESEARCH

4.1. GYRO IMPROVEMENTS AND APPLICATIONS

GYRO Simulations of Missing near Edge L-Mode Transport: While GYRO simulations of core ($0 < r/a < 0.7$) transport (and turbulence intensity) in typical DIII-D L-modes seems to be in good agreement with experiment, it was discover that local GYRO simulated low-k ($k_y\rho_s < 1$) transport and turbulence intensity is about 5-fold lower than experimental levels in a near edge L-mode ($r/a = 0.75$, DIII-D shot 128913.1500). TGLF transport over a large L-mode discharge database indicates that this short fall is not atypical. We recently refocused our efforts on electromagnetic global GYRO simulations of the near edge ($0.7 < r/a < 0.95$) for 128913.1500 and the well-studied 101391.2790. The short fall results mainly because the high near edge electron-ion collisionality stabilizes the TEM modes. Artificially "zeroing" collisions (so χ decreases as $T^{3/2}$) brings back robust near edge transport in both channels. The very high near edge magnetic shear stabilizes the ITG (and TEM) despite the very high logarithmic temperature gradient drives. (The high shear makes for close packing of singular surfaces and challenging GYRO simulations.)

Including higher-k ($k_y\rho_s > 1$) ETG modes can recover much of the experimental electron transport but the short fall in the ion channel remains. The edge transport is highly local because of the very low ρ^*; artificially inducing huge turbulence levels at $r/a > 0.9$ does not reduce the short fall at $r/a = 0.85$ from any significant inward "turbulence spreading". Turning off experimental levels of the $E\times B$ shear does not bring back significant transport. The near edge β is very small so that magnetic flutter transport is negligible.

Inspired by recent GYRO stimulations of NSTX results of very short radial scale micro-tearing modes, we repeated our low-k near edge simulations at very (expensive) short scales ($dx/\rho_s = 0.8 \rightarrow 0.2$ and better resolved singular surfaces) but found no increased transport. This is a disappointment since micro-tearing transport χ is expected to increase like $nT^{-1/2}$ toward a cold high collisional edge. We investigated additional driving mechanisms not found in the standard GYRO formulation but without success (e.g. ionization instability from interaction with edge recycled neutrals; parallel field current gradients). A significant gap in gyro-kinetic transport theory remains.

GYRO Simulations with External Magnetic Perturbations: Working with Franscois Waelbroeck (IFS), we have formulated the GYRO δf code to include model external and static magnetic field perturbations $\Delta\vec{B}_\perp^{ext}$. The motivation is to simulate the effect on transport with respect to the unperturbed toroidally symmetric flux surfaces from the deflection of the parallel magnetic field direction. The model external field of a given low toroidal number n could be tailored to describe external resonant magnetic perturbations (RMPs) or induce a stationary internal magnetic island. The first questions for our initial global GYRO simulations (with and without turbulence driven by plasma gradients) are: (1) what is the

external-field shielding fraction, and (2) does an induced stationary radial electric field $-\nabla_x \delta\phi$ shut down j_x?

After some initial numerical and coding problems, this study of GYRO simulations with external resonant magnetic perturbations has been completed. The results suggest that it may be possible to construct a model to relate the turbulent radial conductivity of an externally isolated island to the radial current flux through the island. $j_r(r)=\sigma^{island} E_r(r_s) T(r,w)$ where $E_r(r_s)$ is the radial electric field at the island. The turbulent radial conductivity σ^{island} can be obtained from the high-n turbulent intensity from TGLF. This gives the torque density from which the Maxwell island stress can be computed. This combined with the Reynolds stress from TGLF can be put into the toroidal angular momentum equation of a transport code to follow the magnetic braking of a rotating plasma from an externally induced island.

To compare and contrast with the isolated island non-ambipolar current flow, we have recently considered GYRO simulations of a region of overlapping island stochastic externally perturbed field lines (similar to error fields from a toroidal field coil current lead). The electrons traveling along stochastic field lines pass island to island "shorting out" the back reaction potential across the whole region and no $E\times B$ transport particle flow is induced, the electrons carry all the radial current (and the ions almost none) via a Rechester-Rosenbluth "magnetic flutter" scaling with the external perturbed field strength like $(\Delta B_r^{ext}/B)^2$. This is in contrast to the isolated island where the peak radial current is independent of $(\Delta B_r^{ext}/B)$ and the ions carry all the current by induced $E\times B$. The radial current spread over the whole region is described by $j_r(r)=\sigma^{stoch}(r)[E_r(r)-E_r^0]$ where the off-set E_r^0 and null torque is much closer to the "electron root" (or electron rest point) E_r.

GYRO Simulations of Electron Transport in Spherical Tokamaks: GYRO simulations of electron transport in spherical tokamaks indicate that electron thermal transport is comparable to that given by experimental analysis, and is dominated by the electromagnetic contribution of electrons free streaming along the stochastic magnetic field lines.

TGYRO/GYRO/NEO Development: The entire TGYRO/GYRO/NEO code suite was moved to revision control under Git and is now hosted at GitHub. Significant reorganization, including new file name conventions, was done, and the Python input parsing code was consolidated and streamlined. This is all in preparation for the GYRO "compact app" component of the CERF center as well as for facilitation of future multi-core code optimization.

New Gyro-kinetic Code Development for Highly Collisional Plasmas: A theoretical formulation for a version of GYRO suitable for the strongly-collisional pedestal region was completed. Development of the new code CGYRO has been started. For the velocity-space coordinates, the code uses the cosine of the pitch angle and the kinetic energy per unit mass for accurate evaluation of the collision operator even for species with disparate masses. Presently a simple Lorentz operator is implemented for the collision dynamics. However, the

code will eventually implement the full linearized gyro-averaged Fokker-Planck collision operator with complete cross-species collisional coupling. Implementation of the collision operator is based on the NEO scheme, i.e. spectral in velocity space with a Legendre series in pitch angle and Laguerre series in energy. The code has been benchmarked with GYRO in the linear, collisionless limit with adiabatic ions for ITG physics. Benchmarks including kinetic electrons and collisions are in progress.

4.2. GYRO ENERGETIC PARTICLE SIMULATIONS

GYRO Energetic-Particle Driven Turbulence: A complete scan of an n=3 reverse shear Alfvén eigenmode (RSAE) frequency sweep has been rendered with the new GYRO GKEIGEN global eigenvalue solver. An interconnected trio of Alfvén eigenmodes, an RSAE, and two toroidal Alfvén eigenmodes (TAEs), are unstable over most of the $q_{\min}$ sweep range of $3.0 \le q_{\min} \le 3.3$ (Fig. 3). Frequencies (neglecting rotation) agree with experiment within about 20%, representing one of the earliest successes in gyro-kinetic simulation of Alfvén eigenmodes. As seen in experiments, the RSAE frequency sweeps upward (and downward), leveling off as it comes near a TAE frequency. Many mode features, including a ubiquitous poloidal shearing, which is absent in MHD but seen in experimental ECE data, and shifted locations of poloidal harmonic peaks, are only detectable with a self-consistent energetic-ion treatment like the one used in this GYRO scan. Preliminary studies of the linear transport "footprint" of Alfvén eigenmodes show that the dominant mode tends to induce transport primarily where local drive is strongest. Transport from some subdominant modes peaks away from local drive. Two mode nonlinear simulations of the discharge are underway.

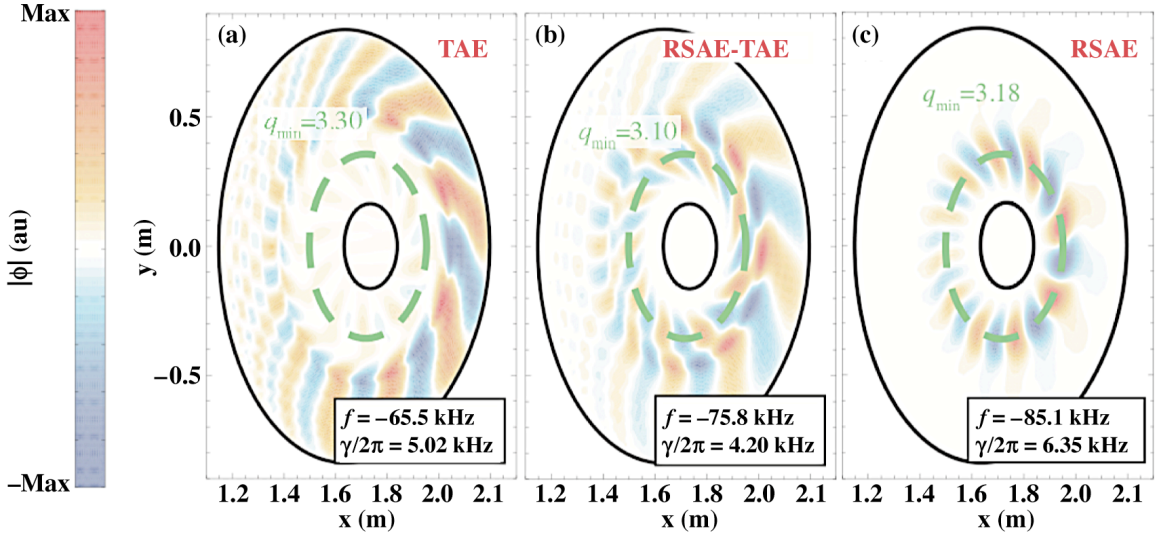

Fig. 3. A poloidal cross section of the electrostatic potential of a simulated (a) TAE, (b) hybrid RSAE-TAE, and (c) RSAE at different values of $q_{\min}$ in DIII-D discharge 142111.

Linear analysis of unstable Alfvén eigenmodes in beam-heated, shear reversed DIII-D discharge 142111 with the GYRO global eigenvalue solver shows at least three distinct, unstable modes (a TAE-RSAE-TAE trio) near t = 725 ms. At least two of these modes can be clearly discerned in the experimental beam emission spectroscopy (BES) spectrogram. At n=3, careful comparison with electron cyclotron emission (ECE) imaging confirms the transition from a single-poloidal-mode-number m RSAE to a two-m TAE (as the minimum in the safety factor $q_{\min}$ evolves with the discharge) in both simulation and experiment. Comparison of the GYRO simulations with results from the gyro-kinetic PIC code GTC and the hybrid MHD and gyro-Landau fluid TAEFL code show nearly identical mode evolution with $q_{\min}$. Frequencies in all three codes agree to within about 20% or better across a single $q_{\min}$ sweep ($3.0 < q_{\min} < 3.3$). Deviation from experimental frequency is consistent with estimated Doppler shift (excluded in all simulations). GYRO and GTC predict similar growth rates; TAEFL growth rates are nearly two times higher. The codes generally agree on mode shearing direction (a "twist" in the mode pattern) near the mode peaks, but disagree in the tail regions. The precise mechanism for this shearing, observed in ECE imaging and simulations, is still under investigation. Gyro-kinetic effects of the beam energetic particles (included self-consistently in the eigenmode calculation) have been suggested, but recent GYRO results seem to preclude this explanation. The level of eigenmode shearing remains constant, as the driving-beam profile is reduced to the point of marginal stability. This suggests an independent mechanism is at work.

4.3. TGLF TRANSPORT MODEL DEVELOPMENT AND VALIDATION

TGLF Transport Model Validation: Predictive modeling using TGLF has shown that stiff core transport is an important ingredient in the prediction of ITER fusion performance. It was recently shown TGLF predicts an ITER fusion gain Q scales as $\beta_{ped}^2/P_{aux}^{0.8}$ in the absence of an input torque, indicating a very stiff core. If the core transport is perfectly stiff, then Q scales like β_{ped}^2/P_{aux}. Perfect core stiffness means that $\beta(0)/\beta_{ped}$ is independent of power throughput. Recent DIII-D and JET experiments validating TGLF have now been shown to operate with comparable core stiffness. By quantifying stiffness, S, as the ratio of the percent change in transported power to the percent change in local temperature gradient, the radial profiles of S from TGLF for DIII-D and JET H-modes used to validate TGLF are found to be comparable to the stiff ITER projection. The stiffness parameter S decreases with increasing radius beyond ρ = 0.5 as the profiles rise increasingly above threshold and the transport spectrum becomes more TEM dominant. For the DIII-D and JET cases shown, near the marginal point ($\rho \sim 0.4$) S is approximately two times larger than what is found near the boundary location (near ρ = 0.8).

A sensitivity study of more than 25 DIII-D L-modes showed that TGLF systematically under-predicts the energy transport in the near edge region. This work is ongoing and the trend continues to hold true for both the electron and ion channels. A comparison was then made to TFTR L-modes. Interestingly, the shortfall in energy transport is much less

pronounced in TFTR compared to DIII-D. While TFTR had circular geometry, this is not believed to be the main cause of the difference. One noticeable difference that is being examined is that the TFTR L-mode edge temperatures are significantly larger than DIII-D L-mode edge temperatures.

TGLF Transport Stiffness: Since core stiffness was found to be an important ingredient in the prediction of the ITER fusion performance, a study was carried out to quantify the stiffness of TGLF in DIII-D L- and H-mode discharges. Here, the focus was on studying the stiffness in various dimensionless scaling experiments defining as the ratio of the percent change in transported power to the percent change in local temperature gradient. For the DIII-D β scans studies, some interesting trends were observed. First, the composite stiffness (change in ion and electron heat flux in response to 10% changes in both the ion and electron temperature gradient) showed no β dependence with stiffness values near 5 at the half radius. Second, a reduction in stiffness was found due to $E\times B$ shear effects from changes in toroidal rotation in the inner core region. Third, stiffness was lower for the β scans performed in the DIII-D shape than for the discharges with the AUG shape.

The current emphasis in this project is the analysis and modeling of the recent DIII-D experiments explicitly designed to study the stiffness of the core transport in H-mode plasmas. Here, low triangularity was utilized to maintain the pedestal height during a series of NBI heated power scans at fixed density and safety factor. Thus far we find that the electrons are very stiff while the ions are moderately stiff (Fig. 4). This is based on observations of the average temperature divided by the temperature at $\rho = 0.84$ (where we place the boundary conditions for TGLF) for the 2 run days.

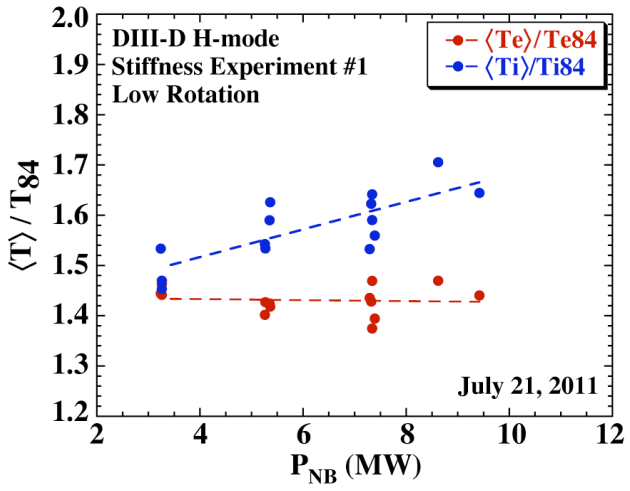

Fig. 4. Variation of volume average temperature divided by the temperature at $\rho = 0.84$ for the electron (red) and ion (blue) temperature versus NBI power for a set of H-mode discharges from a DIII-D stiffness experiment.

TGLF Momentum Transport: The spectral average radial wave number of the nonlinear electric potential from GYRO runs was examined using a new VUGYRO tool. The model for the radial wave number used in TGLF to fit the fluxes and toroidal stress from GYRO $E\times B$ Doppler shear scan was found to be in very good agreement with the spectral

average radial wave number. As expected, the radial wave number shift saturates at large values of the $E\times B$ Doppler shear and the TGLF model was improved to fit this saturation. Additionally, it was found that a pure parallel velocity shear also produces a spectral average radial wave number. This was not unexpected but was hard to deduce from the fluxes alone. A model for TGLF for the radial wave number dependence on the parallel velocity shear was fit to the spectral average results. When both a parallel and a Doppler shear are included together the spectral average radial wave number is approximately the sum of the two individual contributions.

A large number of new GYRO runs were done to examine the parameter dependence of the spectral average radial wave number of the non-linear electric potential using a new tool in VUGYRO. The focus was on the parallel velocity shear induced average radial mode number. A large magnetic shear scan was completed that finds a linear dependence of the radial wave-number on the local mid-plane magnetic shear. There is no q-dependence and the T_i/T_e dependence suggests that the reference frequency is the ion curvature drift frequency (i.e. the average radial wave-number depends upon the ratio of the parallel velocity shear to the ion curvature drift frequency). High mode number runs were done to check the expected reduction of the average radial wave number at high k_y due to FLR gyro-averaging. In parallel to this study of the parallel velocity shear, a study of the average radial wave-number induced by the density and temperature profile shear at larger values than covered in a recent study. The density gradient length shear gives a larger average radial wave number than shear in the temperature gradient length. The goal is to fit a model of the profile shear effects for TGLF but more GYRO runs are needed and the results have been hard to interpret due to the radial profile variation of the fluxes.

4.4. NEOCLASSICAL TRANSPORT AND FLOW

Edge Neoclassical Transport: For various DIII-D H-mode discharges, NEO was used to systematically study finite-orbit-width (FOW) effects due to steep gradients and evaluate the validity of local neoclassical transport in the near-edge region. Three test case discharges were studied: a typical pedestal width and height, a narrow pedestal, and a large pedestal width. For all three cases, no breakdown of local neoclassical theory was observed for quantities that vary on the electron scale such as the electron energy flux, Q_e. Furthermore, local neoclassical theory appears to be valid for the bootstrap current in the near-edge. Only a moderate finite-orbit-width effect was found for the ion energy flux, Q_i. Nonlinear full distribution function (nonlinear-F) simulations may be required for Q_i near the edge for $\Psi_N > 0.93$, but other effects not included here, such as ion orbit loss, may be more important in this region. Regarding the geometry effects, up-down asymmetry flux-surface shaping effects on the non-local transport were found to be weak, but adequate numerical resolution is essential. Specifically, high θ-grid resolution, more than twice the standard resolution, is needed in the edge, due to the strong shaping effects, to prevent artificial enhancement of the FOW effect.

NEO Full Linearized Fokker Planck Collision Operator: The full linearized Fokker-Planck collision operator has been implemented in NEO using new numerical algorithms designed for high-accuracy implicit evaluation for multi-species plasmas, and the effects on neoclassical transport are being studied. The method is based on expanding the distribution function using a Legendre polynomial expansion in the cosine of the pitch angle and a variation of a Laguerre polynomial expansion in normalized velocity. For the latter, the commonly-used Laguerre-based Sonine method was found to yield rapid numerical precision loss, particularly for the high-power elements and for the cross-species field particle matrix elements. The use of quadratic finite elements for the velocity dimension was also found to be too inaccurate to be useful due to the difficulty in obtaining exact ambipolarity due to the lack of exact conservation properties in the energy basis. A combined Laguerre-1/2 + Laguerre-3/2 method was found to be optimal. Convergence to three significant digits can be obtained for modest resolution.

Assessment of Collision Models for Neoclassical Transport: The physical accuracy and limitations of commonly-used model collision operators were studied with the full Fokker-Planck collision operator recently implemented in the NEO code. A comparison of the local neoclassical transport coefficients for model collision operators with the full Fokker-Planck collision operator finds that the zeroth-order Hirshman-Sigmar operator most closely follows the trend of the full Fokker-Planck operator for pure and impure plasmas, except in the highly collisional regime due to missing of the energy exchange effect. While the full Hirshman-Sigmar operator is most accurate for impure plasmas, it is not suitable for experimental analysis since it does not conserve momentum for species with unequal temperatures. A model used in some particle-in-cell codes which consists of the full test particle component but an ad hoc field particle component with simple momentum and energy conserving terms does well in the Pfirsch-Schlüter regime and performs similar to the zeroth-order Hirshman-Sigmar operator in the banana and intermediate collisionality regimes for the energy flux, but is less accurate for the particle fluxes and the bootstrap current. The Connor model is not accurate for impure plasmas due to lack of the deceleration effect.

NEO Experimental Analysis of Neoclassical Transport: A comparison of various model collision operators with the full linearized Fokker-Planck operator for the neoclassical transport for an experimental L-Mode DIII-D case has been studied with NEO. Similar to our previous results, the zeroth-order Hirshman-Sigmar operator generally underestimates the energy fluxes and overestimates the magnitude of the bootstrap current, while the ad hoc field particle operator has the reversed trends. The zeroth-order Hirshman-Sigmar operator also generally underestimates the poloidal flows, while the ad hoc field particle operator underestimates the deuterium ion poloidal flow but overestimates the impurity and electron flows. The results with the ad hoc field particle operator appear to be slightly closer to the experimentally measured value for the impurity poloidal flow, even more so than the results with the full Fokker-Planck operator, though the discrepancies between the numerical results

are small and the difference in the shape of the profiles from the shape of the measured profile suggests that the experimental flow cannot be fully explained by neoclassical processes. Overall, the zeroth-order Hirshman-Sigmar operator seems to better predict the impurity transport coefficients while the ad hoc field particle operator has less error in predicting the deuterium transport coefficients. We would expect the NCLASS results to most closely follow the NEO results using the zeroth-order Hirshman-Sigmar operator since the operator in NCLASS is equivalent. However, there does not appear to be an obvious correlation.

5. ADVANCES IN RF HEATING AND FUELING RESEARCH

5.1. ORBIT-RF AND GENRAY DEVELOPMENTS AND SIMULATIONS

Improvement of ORBIT-RF Monte-Carlo Quasi-Linear Heating Operator: The quasi-linear (QL) heating operator in ORBIT-RF was improved by including the effects due to the change in parallel velocity in the fast Alfvén waves (FW) absorption by particles. Previous QL operator was based on the assumption that particles receive increments only in perpendicular energy when they pass through the cyclotron resonance surfaces. This assumption has been conventionally adapted in the FW heating simulations in present tokamaks. However, it is not strictly correct since FW has finite $k_{\|}$. To be more rigorous, the kick operator in parallel velocity was implemented using a random walk model. Mean change and dispersion terms were derived by extending a previous work by S.C. Chiu based on the Brownian motion theory of individual particles. Previous simulations on DIII-D and NSTX HHFW heating experiments are repeated with the new improved QL heating operator with both "kicks" in parallel velocity and perpendicular energy. However, ORBIT-RF results indicate no significant effect due to the parallel velocity "kick" on the FW absorption by particles, validating the previous assumption that particles receive increments mostly in perpendicular energy.

Improvement of ORBIT-RF Coulomb Collision Operator: Coulomb collision frequencies of a test ion with a background species (drag and pitch angle scattering) vary with the test ion energy. Exact formula that includes Maxwell integral is available to compute these frequencies exactly. But solving Maxwell integral for each test ion at each time step requires significant computational effort when simulations are performed with a large population of test ions over a few slowing down time intervals. Previously, asymptotic expressions for these frequencies are used to speed up the computation. To allow more robust simulations with sufficient computation speed, we tabulate exact collision frequencies by solving Maxwell integral as a function of the ratio of the test ion energy to the background species energy. This table is implemented in ORBIT-RF to allow more accurate calculations of Coulomb collision frequencies of test ions. This improvement in the evaluation of the test-ion collision frequency is not expected to have significant effect on the previous ORBIT-RF DIII-D and NSTX simulation results, since asymptotic expressions are valid for the collision of energetic ions with thermal background ion species. However, in ITER, asymptotic expressions may not be valid since fast ions also collide with fusion born energetic alpha species in the plasma.

ORBIT-RF Simulations of DIII-D High-Harmonic Fast-Wave Experiments: In recent moderate to high harmonic FW heating and current drive experiments in DIII-D, a synergy effect was observed when the 6^{th} harmonic 90 MHz FW is applied to the plasma heated by neutral beams and the 4^{th} harmonic 60 MHz FW. ORBIT-RF was upgraded to

model simultaneous interaction of fast ions with two fast waves. This new version of ORBIT-RF is being applied to simulate these simultaneous interactions of fast ions with two fast waves by comparing simulated synthetic FIDA signals (tangential and vertical) from ORBIT-RF with the measured FIDA data.

GENRAY Improvements: The capability of launching multiple waves with different frequency from each launcher has been added to the general ray tracing code GENRAY. For simulating heating and current drive in GENRAY from lower hybrid (LH) waves or fast waves (FW), multiple grills in the poloidal plane are modeled. In general, each grill can launch a different frequency wave into the plasma, but in the previous version every grill was assumed to launch the same frequency wave. Therefore, to model cases where each grill launches a different frequency, separate simulations were needed for each frequency and the heating and driven current from each grill were summed to compute the total. The upgraded GENRAY code can now launch a different frequency from each grill. Test runs are being done for several cases such as ECCD in ITER, LHCD in FDF, and ICCD and LHCD in ARIES.

5.2. MPI DISRUPTION AND RUNAWAY ELECTRON MITIGATION STUDY

High-Pressure Gas Flow Dynamics in Extended Jet Tubes: The total number of particles delivered to the plasma core before the disruption is terminated can be seriously limited by intrinsic flow rise times during the initial transient-flow phase while the flow asymptotes to steady-state “full flow” conditions. Knowledge of the rise time of the flow in a long delivery tube is an issue for the shutdown dynamics, and especially for creating conditions for strong collisional dissipation of relativistic runaway electrons. Analytical expressions were developed for the time dependence of all gas-dynamic variables, including the gas flow rate at the exit of the gas delivery tube in the ideal frictionless regime. Analytical modeling was compared with 2D asymmetric FLUENT simulations with wall friction, indicating good agreement for sufficiently high conductance pipes in valve-limited flows.

6. ADVANCES IN INTEGRATED MODELING

6.1. IMFIT DEVELOPMENT AND APPLICATIONS

A version of the IMFIT integrated modeling tool was successfully installed at ASIPP-Hefei to support EAST analysis and modeling. A version of the IMFIT integrated modeling code was also successfully installed at IPR-India to support SST-1 analysis and modeling. This version is similar to that installed at ASIPP-Hefei and includes common equilibrium, transport, and stability analysis tasks.

A general IMFIT module driver to drive a Fortran or Python module under the IMFIT framework has been developed and tested. As a first application, a RF heating and current drive GENRAY driver based on this new IMFIT driver has been developed and tested. GENRAY computes power deposition and driven current from RF sources such as lower hybrid (LH), electron cyclotron (EC) and ion cyclotron (IC). Three template input files for use with these three different RF sources have been built and are available in a template directory. GENRAY test runs under IMFIT reproduce very similar results as the standalone GENRAY version.

6.2. ONETWO TRANSPORT CODE DEVELOPMENT

PNFREYA Parallel Neutral Beam Module: Work continued on the implementation of the NFREYA neutral beam module. This is a stand-alone application that can be run independently of any transport code provided that an IMFIT type state file is available. The code newly structured to accommodate an arbitrary number of beamlets in expectation of the 8 beamlines with 4 sources per beamline for DIII-D. Each beamlet consists of a beam and single source. Arbitrary timing of the 32 resulting beamlets is supported. By taking advantage of the parallel nature of the code the only run time penalty incurred is due to the increased number of Monte-Carlo particles required to satisfactorily simulate 32 beamlets. The interface to the transport code ONETWO is through a remote procedure method developed especially so that ONETWO can be run on a single processor machine while multiple calls to PNFREYA may be made on a parallel machine. This approach together with the state file interface means that future inclusion of PNFREYA in other transport codes such as GCNMP is readily accomplished.

ONETWO Development: A new version 5.4 of the ONETWO transport code is ready for release that includes a new parallel version of the neutral beam module PNFREYA and a number of significant enhancements to the ONETWO plasma state file. All known corrections are in place and regression testing was done. One of the primary additions to version 5.4 of the code is the inclusion of the new PNFREYA neutral beam model. In this past quarter, the PNFREYA modules were refined to accommodate the new 14 beam-let experimental setup with 4 individually addressable sources in the 150 degree beam-line and two individual

sources for the remaining beams. The time-dependent beam parameters are taken from an appropriate prepared 14 beam-let UFILE. An output table was created that gives all settings of each source used in the current run. It is expected that this table will be useful for checking the movable beam-line “optics” and can be used to archive the neutral beam injection physics on a shot by shot basis. A significant number of enhancements to the state file were made. This includes all PNFREYA generated neutral beam data.

7. PUBLICATIONS

PRIMARY THEORY AUTHORS FOR 2011

E. Bass and R.E. Waltz, "Gyrokinetic simulation of mesoscale energetic particle-driven Alfvénic turbulent transport embedded in microturbulence," Phys. Plasmas **17**, 112319 (2010).

J. Baumgaertel, E. Belli, W. Dorland, W. Guttenfelder, G. Hammett, D. Mikkelsen, G. Rewoldt, W. Tang, and P. Xanthopoulos, "Simulating Gyro-kinetic Micro-instabilities in Stellarator Geometry with GS2," submitted to Phys. Plasmas.

E. Belli and J. Candy, "Fully Electromagnetic Gyrokinetic Eigenmode Analysis of High-Beta Shaped Plasmas," Phys. Plasmas **17**, 112314 (2010).

E.A. Belli and J. Candy, "Full Linearized Fokker-Planck Collisions in Neoclassical Transport Simulations," submitted to Plasmas Phys. Control. Fusion.

J.A. Boedo, E. Belli, E. Hollmann, W.M. Solomon, D.L. Rudakov, J.G. Watkins, R. Prater, J. Candy, R.J. Groebner, K.H. Burrell, J.S. deGrassie, C.J. Lasnier, A.W. Leonard, R.A. Moyer, G.D. Porter, N.H. Brooks, S. Muller, G. Tynan and E.A. Unterberg, "Poloidally and Radially Resolved Parallel D^+ Velocity Measurements in the DIII-D Boundary and Comparison to Neoclassical Computations," Phys. Plasmas **18**, 032510 (2011).

J. Candy and E.A. Belli, "Neoclassical Transport Including Collisional Nonlinearity," Phys. Rev. Lett. **106**, 235003 (2011).

V.S. Chan, R.D. Stambaugh, A.M. Garofalo, J. Canik, J.E. Kinsey, J.M. Park, M.Y.K. Peng, T.W. Petrie, M. Porkolab, R. Prater, M. Sawan, J.P. Smith, P.B. Snyder, P.C. Stangeby, and C.P.C. Wong, "A Fusion Development Facility on the Critical Path to Fusion Energy," Nucl. Fusion **51**, 083019 (2011).

M. Choi, D.L. Green, V.S. Chan, W.W. Heidbrink, D. Liu, E.F. Jaeger, R.I. Harvey, C.M. Muscatello, L.L. Lao, R.I. Pinsker, and RF-SciDAC Team, "Finite Orbit Monte-Carlo Simulations of Ion Cyclotron Resonant Heating (ICRH) Scenarios in DIII-D, NSTX and ITER," submitted to Nucl. Fusion.

M.S. Chu and M. Okabayashi, "Stabilization of the External Kink and Resistive Wall Mode," Plasmas Phys. Control. Fusion **52**, 123001 (2010).

M.S. Chu, L.L. Lao, M.J. Schaffer, T.E. Evans, E.J. Strait, Y.Q. Liu, M.J. Lanctot, H. Reimerdes, Y. Liu, T.A. Casper, and Y. Gribov, "Response of a Resistive and Rotating Tokamak to External Magnetic Perturbations below the Alfvén frequency," Nucl. Fusion **51**, 073036 (2011).

B.D. Dudson, X.Q. Xu, M.V. Umansky, H.R. Wilson, and P.B. Snyder, "Simulation of Edge Localized Modes Using BOUT++," Plasmas Phys. Control. Fusion. **53**, 054005 (2011).

N.M. Ferraro, S.C. Jardin, and P.B. Snyder, "Ideal and Resistive Edge Stability Calculations with M3D-C1," Phys. Plasmas **17**, 102508 (2010).

N.M. Ferraro, "Symmetries of Resistive Two-Fluid Magnetohydrodynamics under Reversal of Toroidal Field, Current, and Rotation," submitted to Phys. Plasmas 2011.

W. Guttenfelder and J. Candy, "Resolving electron scale turbulence in spherical tokamaks with flow shear," Phys. Plasmas **18**, 022506 (2011).

C. Holland, L. Schmitz, T.L. Rhodes, W.A. Peebles, J.C. Hillesheim, G. Wang, L. Zeng, E.J. Doyle, S.P. Smith, R. Prater, K.H. Burrell, J. Candy, R.E. Waltz, J.E. Kinsey, G.M. Staebler, J.C. DeBoo, C.C. Petty, G.R. McKee, Z. Yan, and A.E. White, "Advances in Validating Gyro-Kinetic Turbulence Models against L- and H-Mode Plasmas," Phys. Plasmas **18**, 056113 (2011).

J.E. Kinsey, G.M. Staebler, J. Candy, R.E. Waltz, and R.V. Budny, "ITER Predictions Using the GYRO Verified and Experimentally Validated TGLF Transport Model," Nucl. Fusion **51**, 083001 (2011).

J.E. Kinsey, G.M. Staebler, and R.E. Waltz "TGLF Transport Modeling of DIII-D Hybrid Discharges," Phys. Plasmas **17**, 122315 (2010).

W.M. Nevins, E. Wang, and J. Candy, "Magnetic Stochasticity in Gyrokinetic Simulations of Plasma Microturbulence," Phys. Rev. Lett. **106**, 065003 (2011).

P.B. Parks and W. Wu, "Limitations of Extended Gas Delivery Tubes Used for Fueling Mitigated Plasma Disruptions and a Unique Injection Concept for Prompt Gas Delivery," Nucl. Fusion **51**, 073014 (2011).

I. Pusztai, J. Candy, and P. Gohil, "Isotop Mass and Charge Effects in Tokamak Plasmas," submitted to Phys. Plasmas.

Q. Ren, M.S. Chu, L.L. Lao, and R. Srinivasan, "High Spatial-Resolution Equilibrium Reconstruction and its Force Balance Analysis," Plasmas Phys. Control. Fusion **53**, 095009 (2011).

P.B. Snyder, R.J. Groebner, J.W. Hughes, T.H. Osborne, M. Buerskens, A.W. Leonard, H.R. Wilson, and X.Q. Xu, "A First Principles Predictive Model of the Pedestal Height and Width: Development, Testing, and ITER Optimization with the EPED Model," Nucl. Fusion **51**, 103016 (2011).

G.M. Staebler and J.E. Kinsey, "Electron Collisions in the trapped gyro-Landau fluid transport mode," Phys. Plasmas **17**, 122309 (2010).

G.M. Staebler, R.E. Waltz, and J.E. Kinsey "Discoveries from the Exploration of Gyro-Kinetic Momentum Transport," Phys. Plasmas **18**, 056106 (2011).

R.D. Stambaugh, V.S. Chan, A.M. Garofalo, M. Sawan, D.A. Humphreys, L.L. Lao, J.A. Leuer, T.W. Petrie, R. Prater, P.B. Snyder, J.P. Smith, and C.P.C. Wong, "Fusion Nuclear Science Facility Candidates," Fusion Sci. Technol. **59**, 279 (2011).

V. Tangri, P.W. Terry, and R.E. Waltz, "A Circular Equilibrium Model for Local Gyrokinetic Simulations of Ion-Temperature Gradient Fluctuations in Reversed Fuel Pinches," accepted for publication in Phys. Plasmas.

A.D. Turnbull, W.A. Cooper, L.L. Lao and Long-Poe Ku, "Ideal MHD Spectrum Calculations for the ARIES-CS Configuration," accepted for publication in Nucl. Fusion 2011.

R.E. Waltz, G.M. Staebler, and W. Solomon, "Gyrokinetic Simulation of Momentum Transport with Residual Stress from Diamagnetic Level Velocity Shears," Phys. Plasmas **18**, 042504 (2011).

R.E. Waltz, and F.L.Waelbroeck, "Gyrokinetic Simulations with External Resonant Magnetic Perturbations: Island Torque and Non-Ambipolar Transport with Rotation," submitted to Phys. Plasmas.

E. Wang, W.M. Nevins, J. Candy, D. Hatch, P. Terry, and W. Guttenfeider, "Electron Heat Transport from Stochastic Fields in Gyro-Kinetic Simulations," Phys. Plasmas **18**, 056111 (2011).

S.K. Wong and V.S. Chan, "Numerical Solution of Neoclassical Ion Transport Using Fokker-Planck Operator for Coulomb Collisions," Plasmas Phys. Control. Fusion **53**, 095005 (2011).

X.Q. Xu, B.D. Dudson, P.B. Snyder, M.V. Umansky, H.R. Wilson, and T. Casper, "Nonlinear ELM Simulations Based on a Nonideal Peeling-Ballooning Model Using the BOUT++ Code," Nucl. Fusion **51**, 103040 (2011).

ACKNOWLEDGMENT

This work supported by the U.S. Department of Energy under Grant No. DE-FG03-95ER54309.